FINITE ELEMENT SIMULATION OF THE BIOMECHANICAL RESPONSE OF THE HUMAN BODY

R. JOST AND G.N. NURICK
Centre for Research in Computational and Applied Mechanics (CERECAM),
Department of Mechanical Engineering, University of Cape Town,
Cape Town, South Africa

ABSTRACT

Described herein is a Finite Element model of the human body for the purpose of simulating damage during vehicle side impact situations. The FE-model consists of the skeleton bones modelled with shell elements and the surrounding soft tissue representing muscles, ligaments and internal organs modelled with solid, membrane and spring-damper elements. Results of the model validation with cadaver sled test data are presented which show satisfactory correlation.

KEY WORDS

Biomedical Response, Human Modelling, Impact

RESEARCH CONDUCTED TO INVESTIGATE the biomechanical impact responses of the human body subjected to lateral impact has been reported by many authors (Eppinger, 1978; Cesari, 1981, 1982; Marcus, 1983; Viano, 1989a, 1989b; Cavanaugh, 1990, 1993; Huang, 1994; Bouquet, 1994; Lizee, 1998). For obvious reasons, tests exceeding injury levels were not performed with living humans and hence human cadavers were used. A pendulum mass was used in impactor tests to impact the cadaver at different body regions with varying initial velocities (Viano, 1989a, 1989b). Sled tests were another test procedure, in which cadavers were impacted against a rigid or padded wall by means of a horizontally accelerated sled (Marcus, 1983; Cavanaugh, 1990, 1993; Huang, 1994). A consequence of the limited number of cadaver tests is that mathematical models have been developed to further investigate the dynamics of the human body in impact tests. One of the most advanced simulation techniques, the Finite Element Method, has been used to examine impact problems in many research fields. The impact effects require dynamic capabilities, thereby adding inertial forces to internal stresses in the structure, requiring more complex material properties and geometry descriptions, and allowing large deformation and self-contact of surfaces. Such models are expensive in preparation and computational time.

The FE-model of the human body described herein consists of all relevant skeletal parts of the human body, the different joints and ligaments that connect the skeletal bones, and displays a high degree of geometrical complexity. All major muscles of the back, neck, abdomen and of the complex shoulder are included in the entire FE-model as separate FE-models, (and are not lumped together as in previous FE-models developed by other authors). Furthermore, three techniques are used to model the different muscle groups. These three different techniques make use of one-dimensional spring-damper elements, two-dimensional membrane elements and three-dimensional solid elements respectively.

MODEL DEVELOPMENT

The model development has been described in more detail by Jost(2001) and is therefore only presented in brief herein: however, to provide some insight into the FE-model the number of elements used are shown in the Appendix. The skeletal bones of the model consist of shell elements that represent only the cortical shell of the bone because cortical bone is about 100 times stiffer than cancellous bone. This is supported by the assumption that the cortical shell contributes most of the stiffness of a bone (Yamada, 1970; Viano, 1986). Muscles are modelled in three different ways. The

simplest is a system of spring-damper-elements placed between the origin and insertion of the muscle. This method considers the force generated by the muscle but does not take into account inertial properties into account. Muscles are also modelled by layers of membrane elements that take into account the mechanical properties more accurately. Additionally these membrane layers can be defined as contact surfaces with other parts of the body. The third approach, which is expensive in preparation and computational time, is the use of solid elements to develop a 3-dimensional model of the muscle geometry as realistically as possible.

SPINAL COLUMN AND THORAX. The skeleton of the back consists of seven cervical, twelve thoracic and five lumbar vertebrae that are connected by intervertebral discs as shown in Figure 1(a). The stability of the vertebral column is provided by the shape and strength of the vertebrae, intervertebral discs, surrounding ligaments and the back muscles. In addition to the strong attachment provided by the intervertebral discs, the vertebrae are united by strong ligaments.

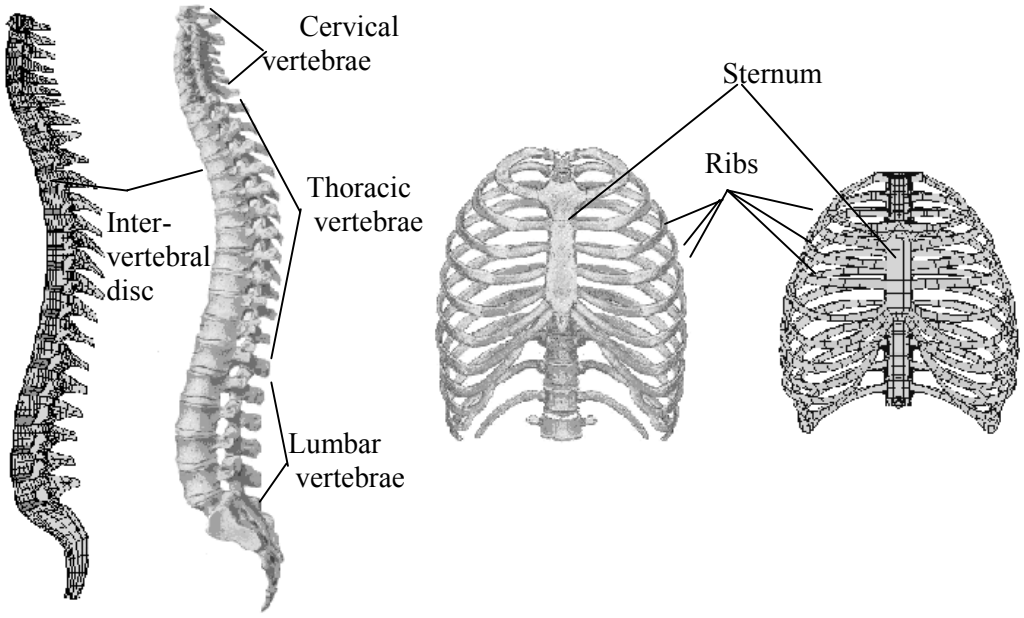

(a) Spinal column (b) Rib cage

Figure 1 - Drawings of anatomical and FE-models of the spinal column and rib cage

The rib cage, depicted in Figure 1(b), is the main skeletal part of the thorax that protects the upper inner organs, heart and the lungs. It consists of 12 ribs that are posteriorly connected to the thoracic vertebrae and anteriorly closed by the costal cartilage and the sternum. The costal cartilage contributes significantly to the flexibility of the rib cage and is modelled by shell elements with cartilage material properties.

MUSCLES OF THE BACK. Behind the spinal column lies a large muscle, the erector spinae that consists of three different layers of smaller muscle groups. The muscle "starts" at the upper surface of the sacrum and is also connected to the inner pelvic wings. The FE-model of the erector spinae follows the curvature of the spine up to the 7^{th} cervical vertebra while it is connected anteriorly at the spinous processes and transverse processes of the lumbar and thoracic vertebrae as shown in Figure 2(a).

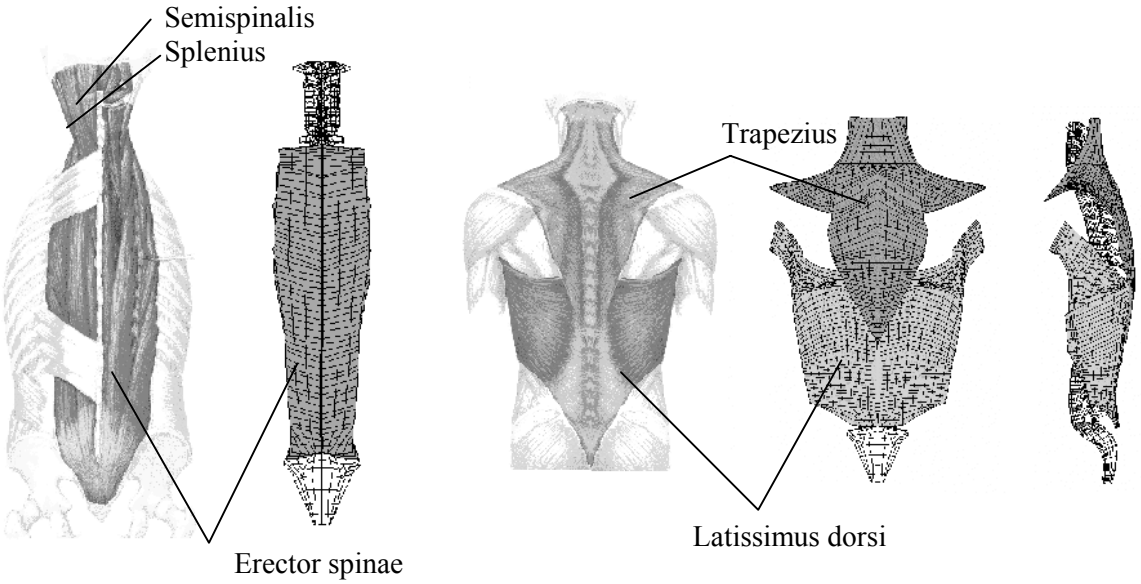

(a) Erector spinae (b) Trapezius and Latissimus dorsi

Figure 2 - Drawings of anatomical and FE-models of the muscles of the back

The second major muscle of the back is the trapezius muscle that covers the upper part of the erector spinae and thoracic spine, shown in Figure 2(b). Another deeper muscle layer is the semispinalis that also runs parallel to the cervical spine and inserts at the back end of the bottom of the skull. These muscles, only briefly presented here, are part of the head-neck complex that has been described in more detail in (Huang, 1994).

THE HEAD – NECK COMPLEX The skeletal part of head-neck complex consists of the skull and seven cervical vertebrae that are connected by intervertebral discs and supporting ligaments. The vertebrae are modelled in the same way as the thoracic vertebrae described earlier while the skull consists of rigid elements. A wide range of movements of the skull is provided by a complex system of joints between the skull and the first two cervical vertebrae. These joints are stabilized by a system of ligaments, represented by layers of membrane elements and spring-damper systems, and the muscles of the neck. In addition to the neck-back muscles described earlier, the sternocleidomastoid muscle is connected to the frontal-upper part of the clavicle and the sternum.

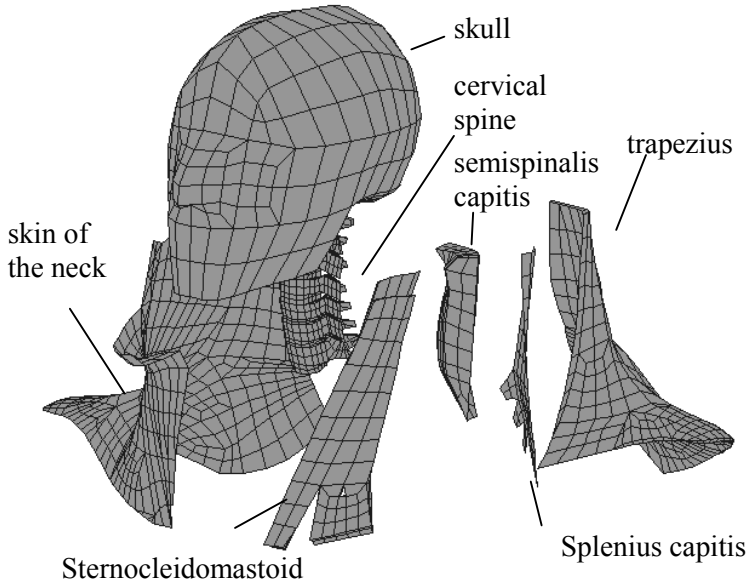

Figure 3 - Drawings of anatomical and FE-models of head and neck

Figure 3 also shows the layers of membrane elements that represent the outer skin of the head-neck complex that serves as a contact surface.

ABDOMEN AND PELVIS The upper part of the abdominal cavity lies within the thoracic cage and its lower part within the wings of the pelvis as shown in Figure 4(a). Anteriorly and laterally it is protected by muscle sheets and posteriorly by thick muscle layers and the spinal column. The skeleton of the pelvis, shown in Figure 4(b), defines the lower border of the abdominal muscles. This is the connection point for many muscles. The bony pelvis is formed laterally by two hip bones, posteriorly by the sacrum and anteriorly by two pubic bones at the pubic symphysis. The sacrum is part of the spinal column and is connected by an intervertebral disc to the first lumbar vertebra. The musculature of the anterior and lateral abdominal wall is composed of a trilaminar sheet consisting of the external and internal oblique muscle and the transversus abdominis muscle. In addition a pair of thick muscles called rectus abdominis, run vertically from the 5^{th}, 6^{th} and 7^{th} costal cartilage above to the insertions of the pubic crest and pubic symphysis of the pelvis.

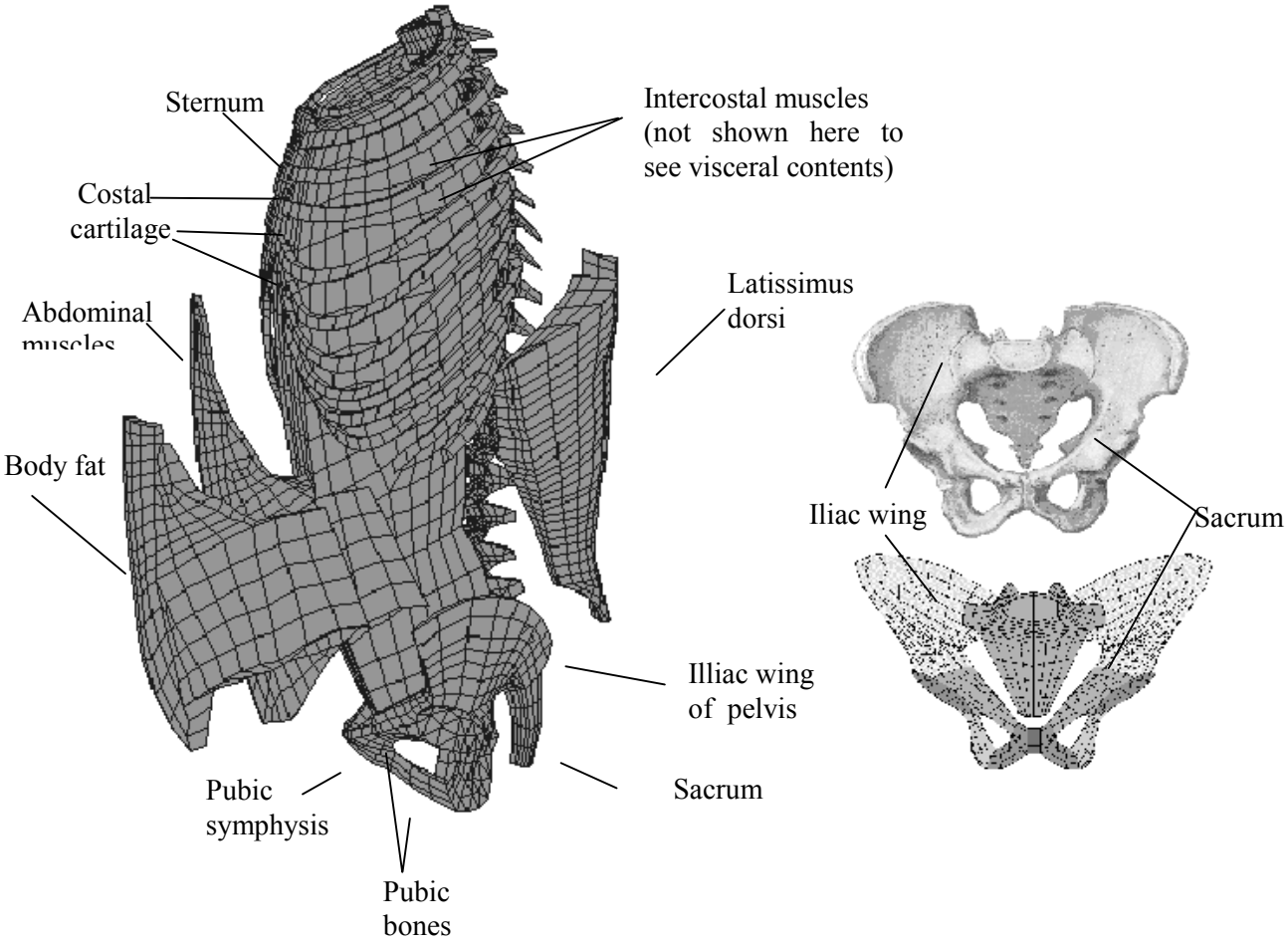

(a) FE-Model of thoracic and abdominal region (b) FE-model of the bony pelvis

Figure 4 – Drawings of anatomical and FE-models of the abdomen and pelvis

All these muscle layers are combined and modelled by muscle elements. The margins of the costal cartilages of the lower ribs and the pubic bones are the attachments of this muscle model. Different material properties for the medial and lateral region take into account the high strength of the rectus abdominis muscles in a vertical direction. Another layer of solid elements is wrapped around this muscle layer to represent some body fat which is relatively easy to change in size and mass.

SHOULDER AND UPPER LIMB The main muscle groups of the arm are the biceps and the triceps. The biceps consist of two parts called long head and short head which are modelled in a simplified manner as shown in Figure 5. The brachialis muscles is part of the biceps model and is directly connected to the humerus. The triceps muscles on the back of the humerus are modelled in a similar way.

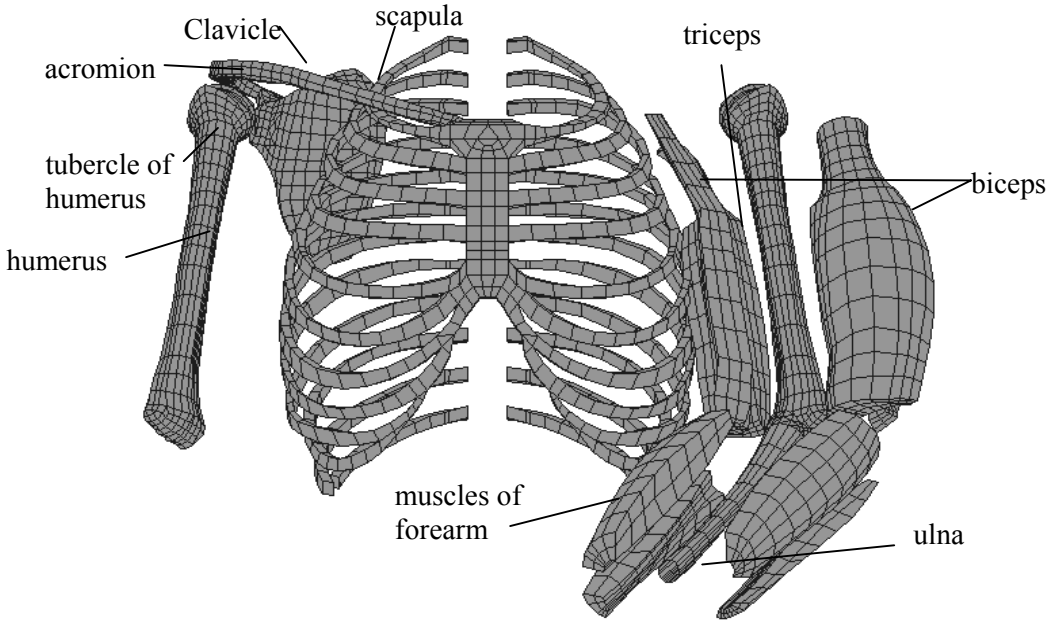

Figure 5 - Drawings of anatomical and FE-models of the rib cage, shoulder bones, arm bone and muscles

The long head of the triceps is connected by membrane elements to the lower margin of the scapula close to the shoulder joint. It joins the short head triceps at the humerus and continues downwards along the shaft of the humerus. The lower ends of the biceps and triceps are simplified at the lower end of the humerus where membrane elements build the bridge over the elbow joint to the ulna of the forearm to stabilise the joint. This model of the elbow joint is a simplification of the real joint but can be justified by the fact that the gross motion of the arm and forearm has been shown to be adequate and also by the fact that injuries of the forearm and elbow joint in side impact have a lower research priority.

The scapula is a flattened, triangular bone that lies on the upper back of the thorax covering parts of the 2nd to 7th ribs. The clavicle connects the scapula with the rib cage at the sternum and the first rib. Modelling of the shoulder is particularly difficult because the scapula is almost free floating on the back of the thorax. This allows for a wide range of movements. Many muscles of the shoulder, shown in Figure 6, are connected to the scapula with complex shapes that are difficult to model. Between the ribs and the scapula lies the serratus anterior and the subscapularis which are of significant importance as they serve as “buffers” in a lateral impact. The subscapularis is a fanshaped muscle which arises from the greater part of the subscapular fossa and passes laterally between the scapula and serratus anterior to converge on a tendon which is attached to the lesser tubercle of the humerus.

On the back of the scapula the infraspinatus arises from the infraspinous fossa of the scapula and is directed towards the shoulder joint and inserts at the greater tubercle of the humerus.

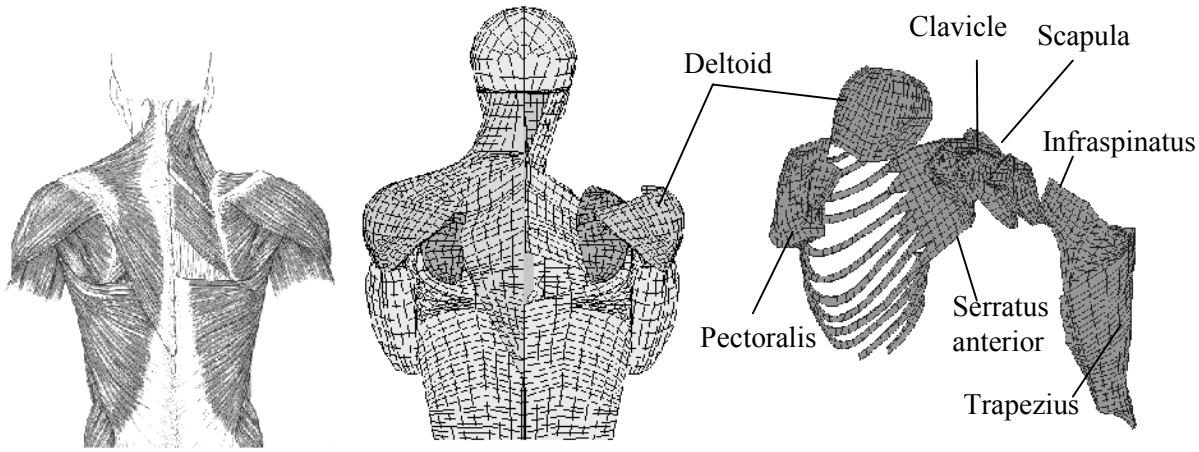

(a) Shoulder muscles and FE-model (b) FE-model of shoulder part

Figure 6 - Drawings of anatomical and FE-models of the muscles and bony parts of shoulder

LOWER LIMBS The thigh, containing the femur, connects the hip and the knee. The leg, containing the tibia and fibula, connects the knee and the ankle that is part of the foot (not shown in Figure 7). The femur is the longest, strongest and heaviest bone of body. The head of the femur is smooth and forms about two-thirds of a sphere and articulates with the acetabulum of the pelvis. The hip joint is a synovial ball socket joint which combines a wide range of movements with high stability. The supporting ligaments that surround the hip joint are simplified by a strong system of spring and damper elements which reduces significantly the complexity of that joint. The tibia and fibula are the bones of the leg of which the tibia supports most of the weight and is for simplification reasons the only bone of the leg modelled. The knee joints are modelled in a similar and simplified way as the elbow joint described earlier with supporting ligaments modelled by membrane elements and a spring-damper system. The musculature of the gluteal region is represented by muscle solid elements that surround the femur and pelvis.

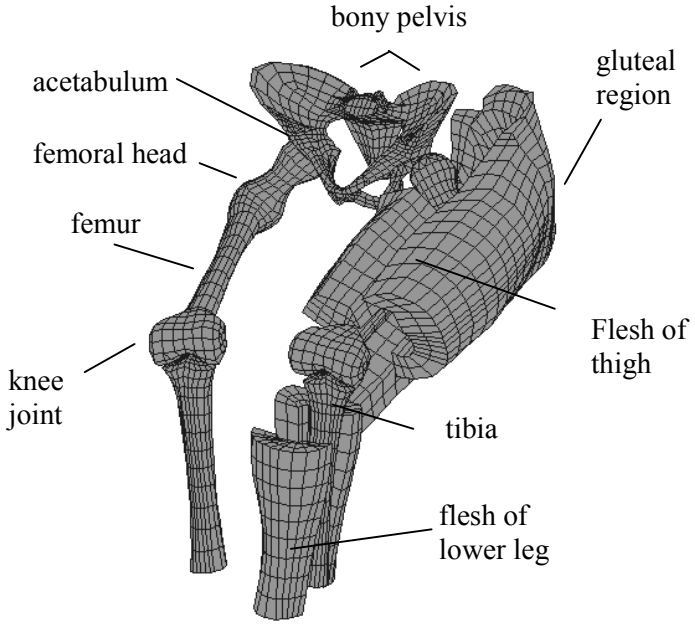

Figure 7 - Drawings of anatomical and FE-models of the skeleton and muscles of the lower limb

No foot model is included but lumped mass elements take account for the relevant mass and inertia.

MODEL VALIDATION - QAULITATIVE OBSERVATIONS

Fundamental biomechanical research in the form of cadaver impactor tests was conducted by (Eppinger, 1978; Cesari, 1981; Viano, 1989a, 1989b; Bouquet, 1994) to investigate the human response to lateral impact. The validation results of the FE-model subjected to these impactor tests have been reported by Jost (2001). A linear impactor makes a localised thoracic impact and can give a direct biomechanical response to the impact, in contrast to cadaver sled test, which simultaneously loads several body regions (shoulder, thorax, abdomen and pelvis), depending on impacted wall topologies. The Heidelberg sled tests (Marcus, 1983) were the first cadaver sled tests to investigate the biomechanical responses of cadavers subjected to lateral impact. Later tests conducted at Wayne State University (Cavanaugh, 1990, 1993; Huang, 1994) had a similar set up. It differed insofar as the impacted wall consisted of four force plates instead of two, as used in the Heidelberg tests. In these tests the human cadavers were initially placed parallel to and approximately 600 to 900 mm from the impacting wall, which is at 90º to the direction of travel of the sled. The sled is gradually accelerated to the test speed, while the offset distance between the cadaver and the wall is maintained. The sled is then rapidly decelerated to zero velocity. The test subjects continue to move over the low-friction ground in the seated position, at the speed of the sled prior to deceleration, towards the wall, which is now stationary. These tests were conducted with initial velocities between 6.5 m/s and 10 m/s. The validation test examples discussed herein are that reported by Cavanaugh (1990, 1993). Figures 8-11 show the cadaver motion subjected to an 8.9 m/s lateral sled test, (recorded as sic04), in comparison to the result of the corresponding response of FE-model.

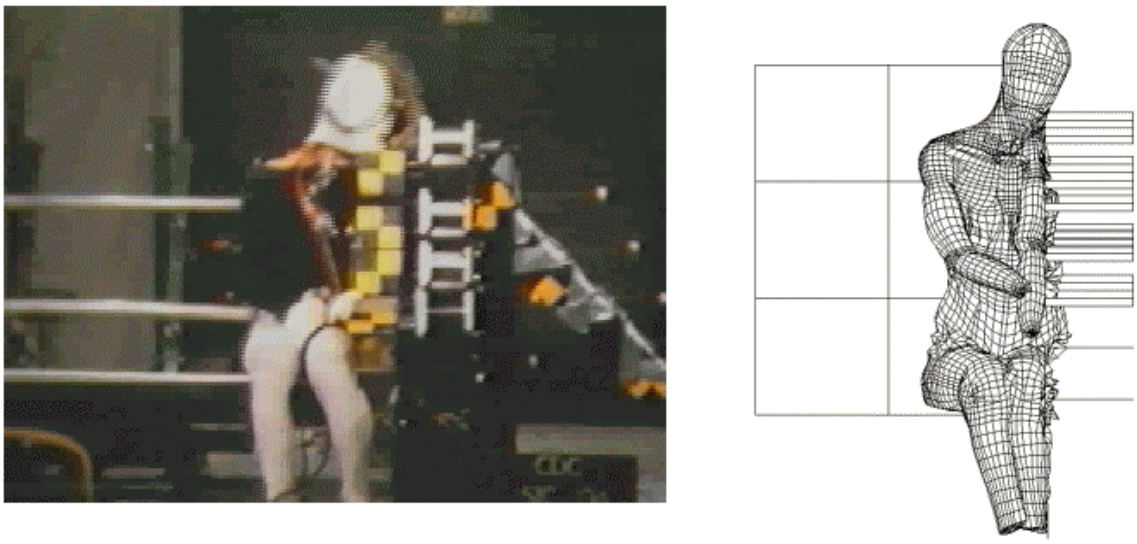

(a) Cadaver (b) FE-model

Figure 8 - Comparison of the photo footage of the impact test in the 8.9 m/s WSU sled test and the FE-model at approximately 25 ms

After about 25 ms the FE-model already shows significant shoulder deformation which is difficult to observe in the cadaver experiment. The legs of the FE-model are already in contact at this stage which cannot be observed in the experiment due to greater initial distance between the legs of the cadaver prior to impact. The head rotation is similar in both cases and is still small at this stage of the impact.

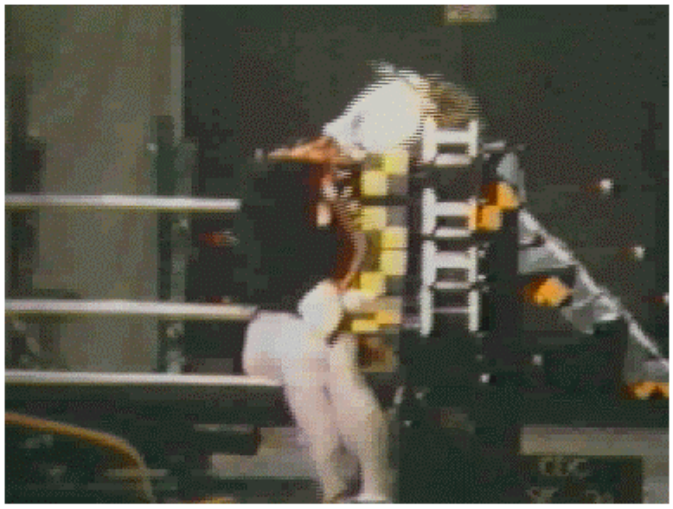

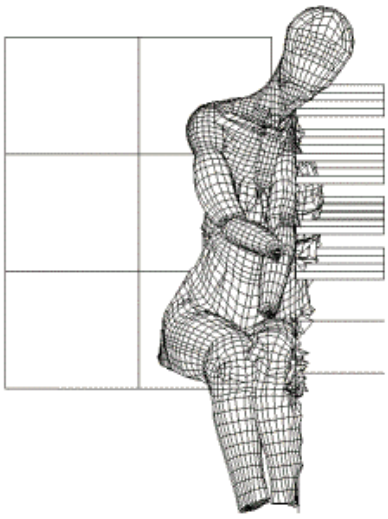

(a) Cadaver (b) FE-model

Figure 9 - Comparison of the photo footage of the impact test in the 8.9 m/s WSU sled test and the FE-model at approximately 40 ms

After about 40 ms, it is assumed that the shoulder of the FE-model penetrates deeper into the thorax than in cadaver case, although it cannot be well observed. The different shoulder deformation probably influences the head rotation, which is less in the case of the FE-model at this stage of the impact. The simulated leg motion correlates well with that observed in the cadaver test.

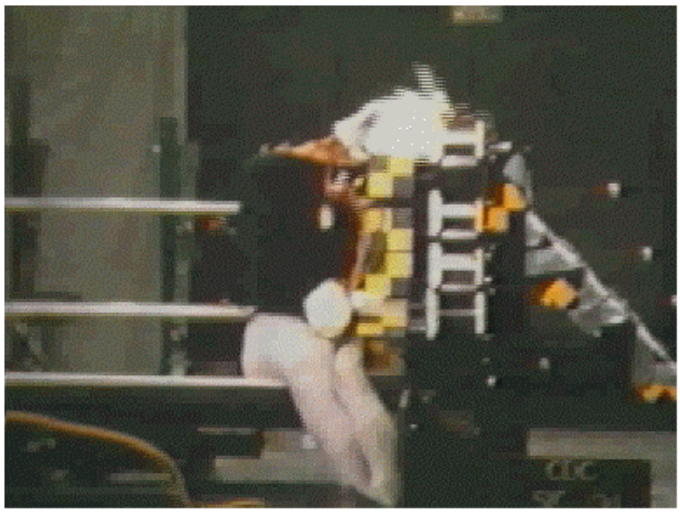

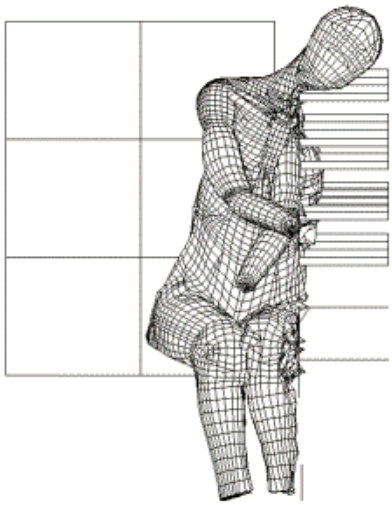

(a) Cadaver (b) FE-model

Figure 10 - Comparison of the photo footage of the impact test in the 8.9 m/s WSU sled test and the FE-model at approximately 45 ms

After about 45 ms almost the entire side of the head of the cadaver impacts the shoulder beam. The head of the FE-model impacts the shoulder beam only at the area of the jaw or chin, which leads to significant strain of the neck. The upper limb of the impacted side of the FE-model is significantly deformed and pushed downwards, which in turn causes the neck to impact the shoulder beam. The

legs of the FE-model have started to bounce off the wall, which cannot be observed in the cadaver test at this stage.

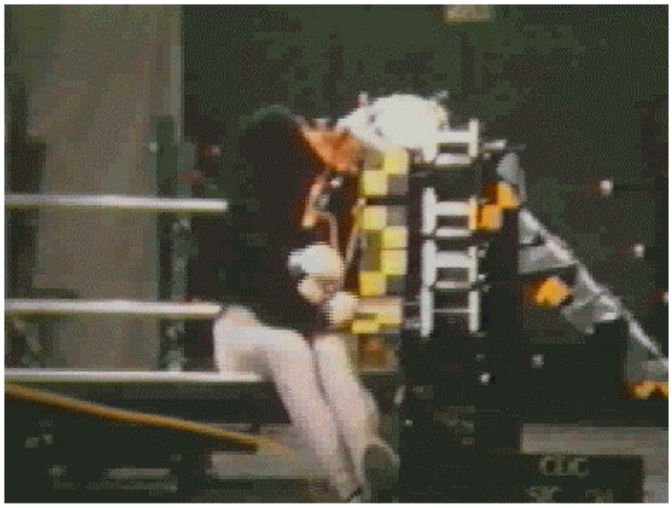

(a) Cadaver

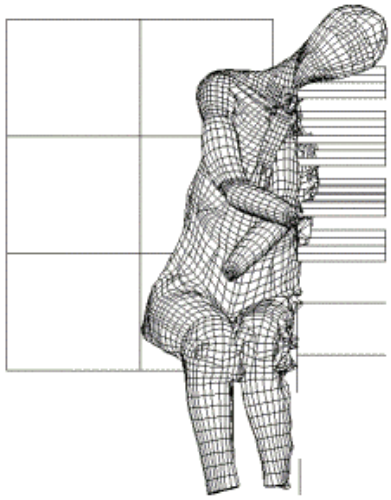

(b) FE-model

Figure 11- Comparison of the photo footage of the impact test in the 8.9 m/s WSU sled test and the FE-model at approximately 55 ms

After about 55 ms the rebounce phase starts. The cadaver does not show the same body rotation around the vertical axis as illustrated in another slower test (6.7 m/s). The head rotation of the FE-model still differs from that observed of the cadaver. The pelvis of the FE-model lifts upwards and the non impacted lower leg of the FE-model bounces off, which does not happen in the cadaver experiment.

The visual comparisons give a first impression that the FE-model behaves similar to the cadaver in the WSU sled tests. This qualitative comparison maybe considered as a first validation step to examine differences in the gross motion of the cadaver and the FE-model. For parameter investigations a quantitative comparison is needed, as for example the comparison of measured force and acceleration responses, and the following section describes a few quantitative comparisons.

MODEL VALIDATION - QUANTATIVE COMPARISON

The first quantitative validation results compare the simulated impact force with the corresponding Heidelberg test result (Marcus, 1983). Figure 12(a) shows the force response corridor that has been developed from the Heidelberg test data for the ISO requirements. Figure 12(b) shows the force response recorded in the WSU sled tests, combining the force-time histories of the shoulder and thoracic beams, since both together cover the same area as the thoracic plate in the Heidelberg tests. The simulated force curve in Figure 12(a) shows a steep rising slope and exceeds slightly the upper border of the experimental response corridor at 5 ms and between 12 ms and 19 ms. The descent of the curve falls within the corridor borders.

The thoracic force in the Heidelberg test is significantly higher than the sum of the thoracic and shoulder force in the WSU test as can be seen in Figures 12(b). The simulated force response shows a similar slope at the beginning as observed in the WSU experiment although it begins 3 ms earlier. The simulated force peak does not reach the experimental value and begins declining earlier. However, the duration of both impacts is almost identical.

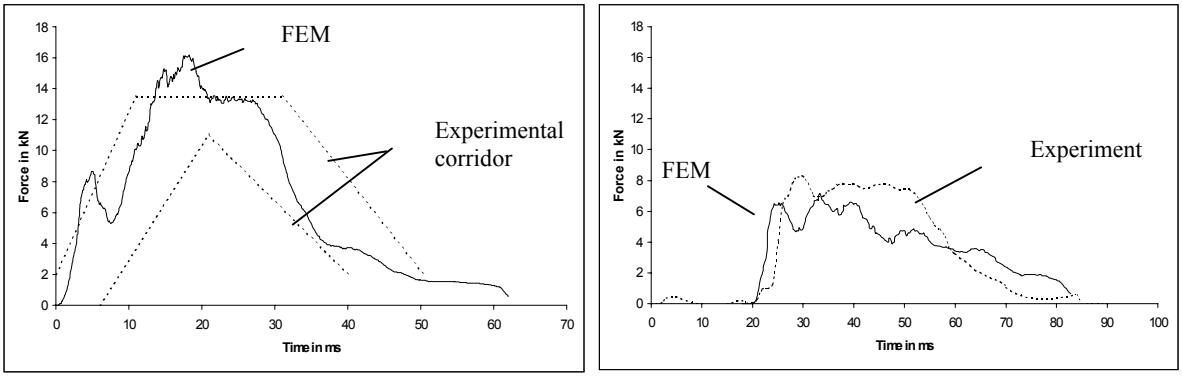

(a) Thoracic force Heidelberg test (b) Thoracic + Shoulder force WSU test

Figure 12 - Diagrams showing comparison of the thoracic cadaver sled test responses at 8.9 m/s

Although the thoracic and shoulder beams cover the same area as the thoracic plate in the Heidelberg test, the peak forces are significantly higher in the latter. It was speculated (Cavanaugh, 1990) that the initial velocities in the Heidelberg tests might have been higher than those in the WSU tests. The comparison between the simulated Heidelberg tests and the simulated WSU tests at the same initial velocity of 8.9 m/s shows the same difference, which has been observed by the comparison of the experimental results of both tests. It might be concluded that the two sled test configurations in fact differ more than originally expected. The results obtained from the FE-model demonstrate that it is sensitive enough to simulate these differences.

The separation of the shoulder and thoracic beams in the WSU tests permits the examination of the thoracic force response with less interference from the shoulder motion. Figure 13 compares the experimental and simulated force responses of the thorax with the WSU tests at 6.7 m/s and 8.9 m/s respectively. For the first 15 ms, until the experimental curve reaches the first maximum value of about 2 kN, the slopes of both curves in Figure 13(a) are almost identical. The simulated curve continues to ascend to ~2.5 kN at 30 ms. It remains at this level until 55 ms, whereafter it declines. The experimental curve displays a similar shape, although the maximum force level of about 2 kN is less than that of the FE-model. The decline of both curves are also similar, both ending at about 80 ms, so that the total thoracic impact lasts for about 60 ms.

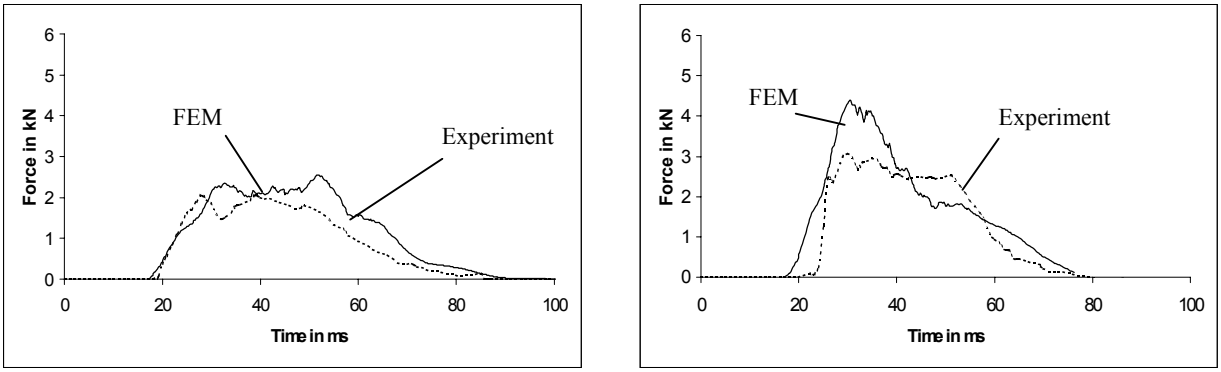

(a) Thoracic force WSU- 6.7 m/s (b) Thoracic force WSU- 8.9 m/s

Figure 13 - Diagrams showing comparison of thoracic WSU responses at two different velocities

For the more severe impact at 8.9 m/s initial velocity, shown in figure 13(b), the simulated force has a distinct peak at about 30 ms, which cannot be observed in the experiment in that form. The simulated force peak value of 4.4 kN exceeds the averaged experimental peak force significantly, with 3.1 kN at 30 ms. However, the shapes of both curves are similar and the force curves do peak at almost the same time. The decline of the simulated curve also closely resembles its experimental counterpart.

CONCLUDING REMARKS

The objective of this work, as also reported in (Jost, 1999, 2000, 2001), was to develop a FE model of the human body for vehicle side impact simulations, with the particular requirement that it was to accurately simulate the biofidelity of the human body. To achieve this objective all the relevant skeletal parts of the human body are modelled by shell elements in greater detail than that reported in previous reported models. The different joints and ligaments of the human body are represented by FE-models of a high geometrical complexity. All major muscles of the back, the neck, the abdomen and the complex shoulder muscles are included as separate FE-models. These model groups interact through contact conditions, which allow for realistic movements among the different muscle layers. Three modelling techniques are applied for the different muscle groups of the body using one-dimensional spring-damper elements, two-dimensional membrane elements and three-dimensional solid elements.

The comparison between the predictions and experiments show a high degree of correlation. In this regard the material properties were utilised to optimise the entire FE-model and not to improve the performance of each particular test. This validation procedure has demonstrated the high level of biofidelity of this FE-model. In addition this model, despite its complexity has proved to operate numerically stable even under severe localised impacts of $9{,}8 ms^{-1}$. The model for the head-neck components was validated for both low and high g-level accelerations (Jost, 2000), which further enhances the biofidelity of the simulations. The simulation indicates that the shoulder dynamics are mainly influenced by the clavicle and deformation of the rib cage, as assumed by Irwin(1993).

While this model has shown suitability for its intended purpose of side impact, several issues need to be further investigated. These include the improvement of the material model for material failure which may cause stability problems because muscle elements, connected to breaking bones, undergo large strains; and the development of visco-elastic materials for muscles and the visceral contents.

For completeness, it would be necessary to include and test this model into a FE-model of a crash vehicle and for other impact directions.

ACKNOWLEDGEMENTS

The authors acknowledge the invaluable support of Professors A. King and J.M. Cavanaugh, Wayne State University, Detroit, USA who kindly provided the experimental sled test data.

REFERENCES

Bouquet, R., Ramet, M., Bermond, F., Cesari, D. Thoracic and pelvic human response to impact, 14th ESV, 94-S1-O-03, 1994.

Cavanaugh, J.M., Zhu, Y., Huang, Y., King, A.I. Injury and response of the thorax in side impact cadaveric tests, 37th Stapp Car Crash Conference, SAE933127, 1993.

Cavanaugh, J.M, Waliko, T.J., Malhotra, A., Zhu, Y., King, A.I. Biomechanical response and injury tolerance of the pelvis in twelve sled side impacts, 34th Stapp Car Crash Conference, SAE902305, 1990.

Cesari, D., Ramet, M., Clair, P. Pelvic tolerance and protection criteria in side impact, 26th Stapp Car Crash Conference, SAE821159, 1982.

Cesari, D., Ramet, M., Bloch J. Influence of arm position on thoracic injuries in side impact, 25th Stapp Car Crash Conference, SAE811007, 1981.

Eppinger, R.H., Augustyn, K., Robbins, D.H. Development of a promising thoracic trauma prediction methodology, 22nd Stapp Car Crash Conference, SAE780891, 1978.

Hall-Craggs, E.C.B. Anatomy, Williams and Willimans Co., Baltimore, 1990.

Huang, Y., King, A., Cavanaugh, J.M. FE modelling of gross motion of human cadavers in side impact, 38th Stapp Car Crash Conference, SAE942207, 1994.

ISO/TR 9790. Road vehicles – anthropomorphic side impact dummy, Part 1-6, 1989.
Irwin, A. and Walilko, T.J. Displacement responses of the shoulder and thorax in lateral sled impacts, 37th Stapp Car Crash Conference, SAE933124, 1993.

Jost, R. and Nurick, G.N. Finite element modelling of the human body in vehicle side impact, International Journal of Crashworthiness, Vol. 4, No.1, 1999, pp 31-37.

Jost, R and Nurick, G.N. Development of a finite element model of the human neck subjected to high g-level deceleration, International Journal of Crashworthiness, 2000. Vol. 5, 2000, pp 259-267.

Jost, R and Nurick, G.N. Finite element simulation of biomechanical response of the human body subjected to lateral impact", International Journal of Crashworthiness, Vol. 6, No1, 2001, pp 123-134.

Lizee, E., Robin, S., Song, E., Bertholon, N., LeCoz, J-Y., Besnault, B., Lavaste, F. Development of a 3d finite element model of the human body, 42nd Stapp Car Crash Conference, SAE983152, 1998, pp.115-138.

Marcus, JH., Morgan, RM., Eppinger, RH., Kallieris, D., Mattern, R., Schmidt, G. Human response to injury from lateral impact, 27th Stapp Car Crash Conference, SAE 831634, 1983.

Viano, D.C., Lau, I.V., Asbury, C., King, A.I., Begeman, P. Biomechanics of the human chest, abdomen and pelvis in lateral impact, 33rd Annual Proceedings of Association for the Advancement of Automotive Medicine, Baltimore, Maryland, 1989.

Viano, D.C, Biomechanical responses and injuries in blunt lateral impact, 33rd Stapp Car Crash Conference, SAE892432, 1989.

Viano, DC, Biomechanics of bone and tissue: a review of material properties and failure characteristics, SAE 861923, 1986.
Yamada, H. Strength of biological materials, The Williams and Wilkins Company Baltimore, 1970.

APPENDIX

Bones		**Joints**			
	Number of shell elements		Number of elements		
			solid	membrane	spring-damper
Back					
T1 – T12	3360	intervert. discs	384	-	96
L1 – L5	1400	-	-	-	-
Thorax					
Ribs	1962	-	-	-	-
Costal cartilage	478	-	-	-	-
Sternum	148	-	-	-	-
Pelvis					
Pelvic bones	1180	-	-	-	-
Sacrum	320	-	-	-	-
Head and Neck					
Headrigid elements	520	-	-	-	-
C1 C2 C3 – C7	162 278 1200	-	-	-	-
Upper Limbs					
Clavicle (each)	588	Shoulder joint (each)			12
Scapula (each)	596	Elbow joint (each)		76	16
Humerus (each)	504	-	-	-	-
Ulna (each)	400	-	-	-	-
Lower Limbs					
Femur (each)	620	Hip joint	-	-	28
Tibia (each)	480	Knee joint	-	-	22

Appendix A1 - Number of elements used for bone and joint models

Muscles			**Ligaments**		
Back	Number of elements		Number of elements		
	solid	membrane		membrane	spring-damper
Erector Spinae	678	128	Supraspinous ligament		48
Trapezius	767	-	Anterior longitudinal ligament	60	-
Latissimus	720	-	ligament flava	60	-
			interspinous ligament	80	-
Thorax					
Intercostal muscles inner + outer layer	-	1144			
Abdomen					-
Rectus abdominis	178	-	Inguinal ligament	86	-
Abdominis muscles	768	-	-	-	-
Fat	318	-	-	-	-
Head and Neck			-	-	-
Spenius capitis	-	128	Cruciform ligament	12	4
Semispinalis capitis	648	-	Alar ligament	18	-
Sternocleidomastoid	192	-	-	-	-
Upper Limbs					
Serratus anterior muscle (each)	324	128	-	-	-
Subscapularis (each)	228	24	-	-	-
Infraspinatus (each)	278		-	-	-
Rhomboid (each)	-	244	-	-	-
Deltoid (each)	648	354	-	-	-
Pectoralis (each)	584	344	-	-	-
Biceps (each)	878	124	-	-	-
Triceps (each)	802	120	-	-	-
Muscles of forearm (each)	380	-	-	-	-
Lower Limbs					
Gluteal region	1948	-	-	-	-
Upper Leg (each)	864	-	-	-	-
Lower Leg (each)	520		-	-	-

Appendix A2 - Number of elements used for muscle and ligament models

	solid elements	membrane elements
Thoracic contents	518	
Heart	120	
Abdominal contents	442	
Pelvic contents	244	
Skin		4800

Appendix A3 - Number of elements used for visceral contents and skin models